

Universität des Saarlandes



Fachrichtung Mathematik

Preprint Nr. 397

BEM-based FEM

Steffen Weißer

Saarbrücken 2017

BEM-based FEM

Steffen Weißer

Saarland University
Department of Mathematics
P.O. Box 15 11 50
66041 Saarbrücken
Germany
`weisser@num.uni-sb.de`

Edited by
FR Mathematik
Universität des Saarlandes
Postfach 15 11 50
66041 Saarbrücken
Germany

Fax: + 49 681 302 4443
e-Mail: preprint@math.uni-sb.de
WWW: <http://www.math.uni-sb.de/>

BEM-based FEM¹

CONTENTS

14.1	Introduction	2
14.2	High-order BEM-based FEM in 2D	3
	14.2.1 Construction of basis functions	4
	14.2.2 Finite Element Method	5
	14.2.3 Introduction to Boundary Element Methods	7
	14.2.4 Numerical examples	8
14.3	Adaptive BEM-based FEM in 2D	9
	14.3.1 Adaptive FEM strategy	10
	14.3.2 Residual-based error estimate for polygonal meshes	11
	14.3.3 Numerical examples	12
14.4	Developments and outlook	15
	14.4.1 Hierarchical construction for 3D problems	15
	14.4.2 Convection-adapted basis functions in 3D	17

THE Boundary Element Method (BEM)-based Finite Element Method (FEM) is an approach to approximate solutions of boundary-value problems over polygonal and polyhedral meshes. The approximation spaces are defined implicitly over the polygonal or polyhedral elements. Harmonic coordinates are recovered for the lowest order approximation in the special case of the diffusion problem. Thus, this method can be viewed as a generalization of harmonic coordinates to higher-order approximations. The definition and treatment of basis functions as well as the finite element formulation are discussed in detail. Furthermore, the BEM-based FEM is applied in the context of an adaptive FEM strategy yielding locally refined polygonal meshes. Theoretical evidence and numerical experiments are presented that establish optimal rates of convergence for uniform and adaptive mesh refinement strategies.

¹This is a pre-publication version of content to appear in *Generalized Barycentric Coordinates in Computer Graphics and Computational Mechanics* (CRC Press, forthcoming 2017. All rights reserved.)

14.1 INTRODUCTION

In this chapter, we study a continuous-Galerkin finite element formulation on polygonal and polyhedral meshes, which is applied to boundary-value problems. The approach was proposed in [2] and established in a sequence of papers [5, 6, 12, 13, 17, 18, 20]. First, the general situation is described in the introduction and afterwards the Poisson problem is considered as a simple model problem to explain the approach.

Let $\Omega \subset \mathbb{R}^d$, $d = 2, 3$ be a bounded polygonal or polyhedral domain with Lipschitz boundary $\partial\Omega = \Gamma_D \cup \Gamma_N$, which is split into a Dirichlet and Neumann part denoted by Γ_D and Γ_N , respectively. We seek to find the function $u : \Omega \rightarrow \mathbb{R}$ that solves the following second order convection-diffusion-reaction boundary value problem:

$$\begin{aligned} Lu = -\operatorname{div}(\mathbf{A}\nabla u) + \mathbf{b} \cdot \nabla u + cu &= f && \text{in } \Omega, \\ u &= g_D && \text{on } \Gamma_D, \\ \frac{\partial u}{\partial \mathbf{n}} &= g_N && \text{on } \Gamma_N, \end{aligned}$$

where \mathbf{n} denotes the outward unit normal vector to Ω . $\mathbf{A} \in \mathbb{R}^{d \times d}$, $\mathbf{b} \in \mathbb{R}^d$, $c \in \mathbb{R}$ are some coefficients, f is a source term and g_D , g_N are boundary data. We assume that the operator L is elliptic and the boundary-value problem has a unique solution. This is guaranteed by the usual assumption on the coefficients and the data.

To obtain an approximation of the unknown solution u , the domain Ω is discretized by non-overlapping polygonal or polyhedral elements and a finite element formulation is applied. The idea of the BEM-based FEM is to use a Trefftz-like approximation space. Its basis functions are defined to fulfil certain local boundary-value problems related to the differential operator L on each element P . In these local problems the coefficients of L are chosen to be constant. The global continuity of the basis functions is ensured by prescribing the boundary data on ∂P . Due to the special choice of basis functions, it is possible to restate the finite element formulation such that only integrals over ∂P appear in the finite element matrix and we do not have to evaluate the basis functions explicitly in the interior of P . However, this procedure involves boundary integral operators, which are treated by means of the BEM in the realization.

All these steps are treated more precisely in the following sections. To simplify the presentation, we restrict ourselves to $L = -\Delta$ and zero Dirichlet data on Γ_D with $|\Gamma_D| > 0$. Thus, we consider the problem

$$-\Delta u = f \text{ in } \Omega, \quad u = 0 \text{ on } \Gamma_D, \quad \frac{\partial u}{\partial \mathbf{n}} = g_N \text{ on } \Gamma_N. \quad (14.1)$$

The well-known variational formulation reads: find $u \in V$ such that

$$b(u, v) = (f, v)_{L_2(\Omega)} + (g_N, v)_{L_2(\Gamma_N)} \quad \forall v \in V, \quad (14.2)$$

where

$$b(u, v) = \int_{\Omega} \nabla u \cdot \nabla v \, d\mathbf{x} \quad \text{and} \quad V = \{v \in H^1(\Omega) : v = 0 \text{ on } \Gamma_D\}.$$

For $f \in L_2(\Omega)$ and $g_N \in L_2(\Gamma_N)$, problem (14.2) admits a unique solution according to the Lax Milgram–Lemma, since the bilinear form $b(\cdot, \cdot)$ is bounded and coercive on V . To obtain a discrete finite element solution we replace V in (14.2) by a finite-dimensional conforming subspace $V_h \subset V$ that is spanned by some basis functions, i.e., $V_h = \text{span}\{\varphi_1, \dots, \varphi_m\}$. The ansatz $u_h = \sum_{i=1}^m u_i \varphi_i$ yields the finite element system of linear equations

$$\mathbf{K}\mathbf{u} = \mathbf{f} \quad \text{for } \mathbf{u} = (u_1, \dots, u_m) \in \mathbb{R}^m, \quad (14.3)$$

where

$$\mathbf{K} = (b(\varphi_j, \varphi_i))_{i,j=1}^m \in \mathbb{R}^{m \times m}, \quad \mathbf{f} = ((f, \varphi_i)_{L_2(\Omega)} + (g_N, \varphi_i)_{L_2(\Gamma_N)})_{i=1}^m \in \mathbb{R}^m.$$

The basis functions φ_i are defined over the polygonal or polyhedral mesh \mathcal{T}_h in such a way that they have local support. Consequently, the finite element stiffness matrix \mathbf{K} is sparse, and it is symmetric as well as positive definite because of the properties of $b(\cdot, \cdot)$. Therefore, efficient numerical solvers such as those based on the conjugate gradient method are available to solve (14.3).

In the first part of this chapter we consider the two-dimensional case $d = 2$. We already mentioned that the basis functions φ_i are defined locally on each polygonal element P with the help of the differential operator $L = -\Delta$ in the BEM-based FEM. For the first-order approximation space we prescribe linear data on ∂P and use $-\Delta\varphi_i = 0$ in P . Obviously, we recover harmonic coordinates that were first proposed in [10] for applications in Computer Graphics, see Section 1.2.8 too. These harmonic coordinates belong to the class of generalized barycentric coordinates which also find applications in polygonal finite element methods, see Chapter 11. The general construction of basis functions for high-order approximation spaces within the BEM-based FEM is discussed in Section 14.2. This approach generalizes harmonic coordinates to higher order basis functions and shows similarities to the Virtual Element Method (VEM). The VEM was first introduced in [1] and is discussed in Chapter 15. In Section 14.2, we additionally discuss the treatment of the locally implicit basis functions and the computation of the finite element matrix \mathbf{K} . This involves the applications of BEM locally, for which we give a short introduction. One of the promising application areas of polygonal meshes is in adaptive mesh refinement, where the flexibility of using different element shapes in the meshes can be exploited. In Section 14.3, an adaptive FEM strategy is reviewed which makes use of the BEM-based FEM and a residual-based a-posteriori error estimator. Numerical experiments are presented that demonstrate the applicability of using polygonal meshes to solve two-dimensional boundary-value problems. Finally in Section 14.4, we present an outlook to further developments in 2D and 3D.

14.2 HIGH-ORDER BEM-BASED FEM IN 2D

In this section, we address the finite element formulation and give theoretical and numerical rates of convergence for the BEM-based FEM on sequences of uniformly

4 ■ Generalized Barycentric Coordinates in Computer Graphics and Computational Mechanics

refined meshes. First, the domain $\Omega \subset \mathbb{R}^2$ is decomposed into a finite number of non-overlapping polygonal elements P such that $\bar{\Omega} = \bigcup\{\bar{P} : P \in \mathcal{T}_h\}$. Here, \mathcal{T}_h is the set of all these polygonal elements, and it is called the polygonal mesh. We assume that \mathcal{T}_h is regular, i.e., all polygonal elements $P \in \mathcal{T}_h$ are star-shaped with respect to a circle such that the aspect ratio h_P/ρ_P of their diameter h_P and the radius ρ_P of the circle is uniformly bounded for all elements, and that the lengths $h_{[\mathbf{v}_i, \mathbf{v}_{i+1}]}$ of the edges of P can be uniformly bounded from below such that $c_{\mathcal{T}}h_P \leq h_{[\mathbf{v}_i, \mathbf{v}_{i+1}]}$ for a fixed constant $c_{\mathcal{T}}$.

14.2.1 Construction of basis functions

The global approximation space $V_h = \text{span}\{\varphi_1, \dots, \varphi_m\}$ is also denoted by V_h^k to specify its approximation order $k \in \mathbb{N}$. It is constructed by prescribing its basis functions φ_i over the single elements $P \in \mathcal{T}_h$ such that

$$V_h^k = \{v \in V : v|_P \in V_h^k(P) \forall P \in \mathcal{T}_h\},$$

and we only have to give a local basis for $V_h^k(P)$.

Let $\mathcal{P}^k(\omega)$ be the space of polynomials of degree less than or equal to k over ω , where ω is either an element P or an edge $[\mathbf{v}_i, \mathbf{v}_{i+1}]$. Before we address $V_h^k(P)$, we introduce an auxiliary space over ∂P . Let

$$\mathcal{P}_{\text{pw}}^k(\partial P) = \{v \in C(\partial P) : v|_{[\mathbf{v}_i, \mathbf{v}_{i+1}]} \in \mathcal{P}^k([\mathbf{v}_i, \mathbf{v}_{i+1}]), i = 1, \dots, n\}$$

be the space of piecewise functions on ∂P which are polynomials of degree smaller or equal to k over each edge $[\mathbf{v}_i, \mathbf{v}_{i+1}]$ and which are continuous at the vertices \mathbf{v}_i . Furthermore, let $\{\lambda_i : i = 1, \dots, kn\}$ be a basis set of $\mathcal{P}_{\text{pw}}^k(\partial P)$, where λ_i , $i = 1, \dots, n$ is linear on each edge $[\mathbf{v}_j, \mathbf{v}_{j+1}]$ and fulfils $\lambda_i(\mathbf{v}_j) = \delta_{ij}$. For $i > n$, λ_i are chosen as polynomial bubble functions that vanish at the vertices and have local support on one edge. For example, λ_i , $i = n + 1, \dots, 2n$ is a quadratic polynomial over $[\mathbf{v}_i, \mathbf{v}_{i+1}]$, λ_i , $i = 2n + 1, \dots, 3n$ is a cubic polynomial over $[\mathbf{v}_i, \mathbf{v}_{i+1}]$, and so on.

Next, the space $V_h^k(P)$ is given by prescribing its basis functions. They satisfy certain boundary-value problems on P , as mentioned in the introduction. Since $L = -\Delta$ in the model problem, we define ϕ_i , $i = 1, \dots, kn$ as the unique solution of

$$-\Delta\phi_i = 0 \quad \text{in } P \quad \text{and} \quad \phi_i = \lambda_i \quad \text{on } \partial P. \quad (14.4)$$

For the lowest-order case $k = 1$, we recover harmonic coordinates, compare Section 1.2.8. For $k > 1$, we have additional harmonic basis functions with polynomial data on ∂P . Furthermore, we introduce element bubble functions $\phi_{i,j}$ for $k > 1$ with $i = 0, \dots, k - 2$ and $j = 0, \dots, i$ as the unique solutions of

$$-\Delta\phi_{i,j} = p_{i,j} \quad \text{in } P \quad \text{and} \quad \phi_{i,j} = 0 \quad \text{on } \partial P, \quad (14.5)$$

where $p_{i,j}(\mathbf{x}) = (x - \bar{x})^{i-j}(y - \bar{y})^j$ and $\bar{\mathbf{x}} = (\bar{x}, \bar{y})$ is the center of mass of P . Later on, it is convenient to reformulate the local boundary-value problems for the element

bubble functions $\phi_{i,j}$ such that they reduce to Laplace problems. Afterwards, $\phi_{i,j}$ can be expressed in terms of the harmonic basis functions ϕ_i . This yields the form

$$\phi_{i,j} = q_{i,j} - \sum_{\ell=1}^n \alpha_\ell \phi_\ell, \quad (14.6)$$

where $q_{i,j} \in \mathcal{P}^k(P)$ is such that $-\Delta q_{i,j} = p_{i,j}$. The polynomial $q_{i,j}$ is always constructible and it is not unique. The coefficients α_ℓ are chosen in accordance with $q_{i,j}|_{\partial P} - \sum_{\ell=1}^n \alpha_\ell \lambda_\ell = 0$.

Since the basis functions are defined as solutions of boundary-value problems, the theory of partial differential equations provides regularity results. It is known that the solution of (14.4) and (14.5) belongs to $C^2(P) \cap C(\bar{P})$ for convex elements P . In the case of non-convex elements the classical smoothness is lost and the differential equations have to be understood in the weak sense. Nevertheless, the basis functions still belong to $H^1(P) \cap C(\bar{P})$, which is sufficient to ensure conformity.

Finally, the space $V_h^k(P)$ is defined as the span of the functions ϕ_i and $\phi_{i,j}$. Since $\{p_{i,j} : i = 0, \dots, k-2 \text{ and } j = 0, \dots, i\}$ is a basis set of $\mathcal{P}^{k-2}(P)$, we obtain

$$V_h^k(P) = \{v \in H^1(P) : -\Delta v \in \mathcal{P}^{k-2}(P) \text{ and } v|_{\partial P} \in \mathcal{P}_{\text{pw}}^k(\partial P)\}. \quad (14.7)$$

Furthermore, we observe that $\mathcal{P}^k(P) \subset V_h^k(P)$. This is a consequence of the unique solvability of the Poisson problem with Dirichlet boundary data. For $p \in \mathcal{P}^k(P)$, it is evidently $p|_{\partial P} \in \mathcal{P}_{\text{pw}}^k(\partial P)$ and $-\Delta p \in \mathcal{P}^{k-2}(P)$ and thus $p \in V_h^k(P)$.

The VEM in Chapter 15 also uses the local space defined in (14.7). Therefore, the BEM-based FEM and the VEM seek the approximation of the solution of the boundary-value problem for the Poisson equation (14.1) in the same discrete space. The VEM reduces all computations to carefully chosen degrees of freedom and to local projections into polynomial spaces. The BEM-based FEM in contrary makes use of the explicit knowledge of the basis functions and thus enables the evaluation of the approximation inside the elements. Both methods rely on clever reformulations to avoid volume integration. Since the BEM-based FEM applies Trefftz-like basis functions, which are related to the differential equation of the global problem, the discrete space for the BEM-based FEM and the VEM differ as soon as more general boundary-value problems are considered.

14.2.2 Finite Element Method

The conforming approximation space $V_h^k \subset H^1(\Omega)$ can be utilized in a FE computation. The variational formulation of the model problem is already given in (14.2) and its approximation yields the system of linear equations (14.3). The approximation properties of the Galerkin formulation have been studied in [12, 18]. The space V_h^k yields the same error estimates that are known for classical approximation spaces over triangulations, but on much more general meshes.

Theorem 14.1. *Let \mathcal{T}_h be a regular polygonal mesh, $u \in V$ be the solution of (14.2) and $u_h \in V_h^k$ be the Galerkin approximation obtained by (14.3). Then,*

$$\|u - u_h\|_{H^\ell(\Omega)} \leq c h^{k+1-\ell} |u|_{H^{k+1}(\Omega)} \quad \text{for } u \in H^{k+1}(\Omega) \text{ and } \ell = 0, 1,$$

6 ■ Generalized Barycentric Coordinates in Computer Graphics and Computational Mechanics

where the constant c only depends on the mesh regularity and for $\ell = 0$ some additional regularity of the dual problem is assumed.

It remains to discuss the setup of (14.3) and how to compute the involved integrals. The setup of the matrix \mathbf{K} and the right hand side \mathbf{f} is done as usual in FEM by agglomerating local (element-wise) stiffness matrices. Therefore, we write

$$b(\varphi_j, \varphi_i) = \sum_{P \in \mathcal{T}_h} \int_P \nabla \varphi_i \cdot \nabla \varphi_j \, d\mathbf{x}. \quad (14.8)$$

The difficulty arises in the application of the bilinear form to the implicitly defined basis functions and to evaluate the integral $(f, \varphi_i)_{L_2(P)}$ on the right hand side. The computation of the boundary integral $(g_N, \varphi_i)_{L_2(\Gamma_N)}$ is straightforward, since the basis functions φ_i are known explicitly along the edges. Thus, these integrals are treated over each edge in Γ_N by numerical quadrature.

To evaluate the integrals in (14.8), we distinguish three cases and apply Green's first identity locally on each element $P \in \mathcal{T}_h$. The details are left to the reader. If $\varphi_i|_P$ and $\varphi_j|_P$ correspond to harmonic basis functions ϕ_i and ϕ_j , we obtain

$$\int_P \nabla \phi_i \cdot \nabla \phi_j \, d\mathbf{x} = \int_{\partial P} \frac{\partial \phi_i}{\partial \mathbf{n}_P} \phi_j \, ds_{\mathbf{x}}. \quad (14.9)$$

If $\varphi_i|_P$ and $\varphi_j|_P$ correspond to element bubble functions $\phi_{i,j}$ and $\phi_{i',j'}$, we obtain with the representation (14.6)

$$\int_P \nabla \phi_{i,j} \cdot \nabla \phi_{i',j'} \, d\mathbf{x} = \int_{\partial P} \frac{\partial q_{i,j}}{\partial \mathbf{n}_P} q_{i',j'} \, ds_{\mathbf{x}} - \sum_{\ell=1}^n \alpha_\ell \int_{\partial P} \frac{\partial \phi_\ell}{\partial \mathbf{n}_P} q_{i',j'} \, ds_{\mathbf{x}} + \int_P p_{i,j} q_{i',j'} \, d\mathbf{x}.$$

And if $\varphi_i|_P$ corresponds to a harmonic basis function and $\varphi_j|_P$ to an element bubble functions, we obtain $\int_P \nabla \varphi_i \cdot \nabla \varphi_j \, d\mathbf{x} = 0$. Therefore, the system of linear equations decouples in the FE computation. Furthermore, besides the unknown term $\partial \phi_i / \partial \mathbf{n}_p$ all others are (piecewise) polynomials such that the first and third integral in the last formula can be analytically computed. The approximation of $\partial \phi_i / \partial \mathbf{n}_p$ is addressed in the next subsection.

For the computation of $(f, \phi_i)_{L_2(\Omega)}$, we proceed as in (14.8). Then, we approximate the local integrals $\int_P f \varphi_i \, d\mathbf{x}$ by a numerical quadrature over polygonal elements. This is realized by subdividing the polygon into triangles and applying standard quadrature rules over them, cf. [15]. Alternatively, we might also apply quadrature rules over polygons directly, see for example [11]. If $\varphi_i|_P$ corresponds to a harmonic basis function ϕ_i , we make use of the representation formula

$$\phi_i(\mathbf{x}) = -\frac{1}{2\pi} \int_{\partial P} \ln |\mathbf{x} - \mathbf{y}| \frac{\partial \phi_i(\mathbf{y})}{\partial \mathbf{n}_P} \, ds_{\mathbf{y}} - \frac{1}{2\pi} \int_{\partial P} \frac{\mathbf{n}_P \cdot (\mathbf{x} - \mathbf{y})}{|\mathbf{x} - \mathbf{y}|^2} \phi_i(\mathbf{y}) \, ds_{\mathbf{y}} \quad (14.10)$$

for $\mathbf{x} \in P$, see below. If $\varphi_i|_P$ corresponds to an element bubble function, we apply (14.6). We stress again that the knowledge of $\partial \phi_i / \partial \mathbf{n}_p$ is important.

14.2.3 Introduction to Boundary Element Methods

The representation formula (14.10) is crucial for boundary element methods which are utilized to approximate boundary integral formulations. To be mathematically precise, see [14], we denote by $\gamma_0 : H^1(P) \rightarrow H^{1/2}(\partial P)$ the usual trace operator that satisfies $\gamma_0 v = v|_{\partial P}$ for continuous functions. Furthermore, let $\gamma_1 v \in H^{-1/2}(\partial P)$ be the conormal derivative, also called Neumann trace, of a function $v \in H^1(\Omega)$ with Δv in the dual of $H^1(\Omega)$. The Neumann trace $\gamma_1 v$ is defined by Green's identity

$$\int_P \nabla v \cdot \nabla w \, d\mathbf{x} = \int_{\partial P} \gamma_1 v \, \gamma_0 w \, ds_{\mathbf{x}} - \int_P w \Delta v \, d\mathbf{x}$$

for $w \in H^1(P)$ and coincides with $\partial v / \partial \mathbf{n}_P$ for sufficient regular functions. Thus, we write (14.10) in terms of boundary integral operators for a harmonic function v as $v = \mathcal{V}(\gamma_1 v) - \mathcal{W}(\gamma_0 v)$ in P . Applying the trace operators γ_0 and γ_1 to the representation formula yields the Calderon projector

$$\begin{pmatrix} \gamma_0 v \\ \gamma_1 v \end{pmatrix} = \begin{pmatrix} \frac{1}{2}\mathcal{I} - \mathcal{K} & \mathcal{V} \\ \mathcal{D} & \frac{1}{2}\mathcal{I} + \mathcal{K}' \end{pmatrix} \begin{pmatrix} \gamma_0 v \\ \gamma_1 v \end{pmatrix}, \quad (14.11)$$

where \mathcal{I} is the identity operator. The single layer, double layer and adjoint double layer potential as well as the hypersingular integral operator have the mapping properties

$$\begin{aligned} \mathcal{V} : H^{-1/2}(\partial P) &\rightarrow H^{1/2}(\partial P), & \mathcal{K} : H^{1/2}(\partial P) &\rightarrow H^{1/2}(\partial P), \\ \mathcal{K}' : H^{-1/2}(\partial P) &\rightarrow H^{-1/2}(\partial P), & \mathcal{D} : H^{1/2}(\partial P) &\rightarrow H^{-1/2}(\partial P). \end{aligned}$$

For a detailed study of these operators see [14]. The first equation in (14.11) gives the boundary integral equation $\mathcal{V}(\gamma_1 v) = (\frac{1}{2}\mathcal{I} + \mathcal{K})(\gamma_0 v)$. Consequently, if $\gamma_0 v$ is known, the Neumann trace $t = \gamma_1 v$ is given as the solution of the Galerkin formulation

$$(\mathcal{V}t, \tau)_{L_2(\partial P)} = ((\frac{1}{2}\mathcal{I} + \mathcal{K})\gamma_0 v, \tau)_{L_2(\partial P)} \quad \forall \tau \in H^{-1/2}(\partial P).$$

This formulation admits a unique solution, since \mathcal{V} is known to be invertible for $h_P < 1$. To obtain an approximation of $t \in H^{-1/2}(\partial P)$, we apply the BEM. We discretize $H^{1/2}(\partial P)$ by $\mathcal{P}_{\text{pw}}^k(\partial P)$ and $H^{-1/2}(\partial P)$ by $\mathcal{P}_{\text{pw,d}}^{k-1}(\partial P)$, where

$$\mathcal{P}_{\text{pw,d}}^{k-1}(\partial P) = \{v \in L_2(\partial P) : v|_{[\mathbf{v}_i, \mathbf{v}_{i+1}]} \in \mathcal{P}^{k-1}([\mathbf{v}_i, \mathbf{v}_{i+1}]), i = 1, \dots, n\}$$

is the space of piecewise polynomials of order smaller or equal to $k-1$ that allow discontinuities at the vertices of P . Let $\{\tau_i : i = 1, \dots, kn\}$ be a basis set of $\mathcal{P}_{\text{pw,d}}^{k-1}(\partial P)$ which is constructed analogously to $\{\lambda_i : i = 1, \dots, kn\}$. For polynomial data $\gamma_0 v = \sum_{i=1}^{kn} v_i \lambda_i \in \mathcal{P}_{\text{pw}}^k(\partial P)$, the ansatz $t \approx t_h = \sum_{i=1}^{kn} t_i \tau_i \in \mathcal{P}_{\text{pw,d}}^{k-1}(\partial P)$ yields the system of linear equations

$$\mathcal{V}t = (\frac{1}{2}\mathcal{M} + \mathcal{K})v, \quad (14.12)$$

8 ■ Generalized Barycentric Coordinates in Computer Graphics and Computational Mechanics

with $\mathbf{t} = (t_1, \dots, t_{kn})$ and $\mathbf{v} = (v_1, \dots, v_{kn})$, where

$$\begin{aligned}\mathbf{V} &= \left((\mathcal{V}\tau_j, \tau_i)_{L_2(\partial P)} \right)_{i,j=1}^{kn}, & \mathbf{M} &= \left((\lambda_j, \tau_i)_{L_2(\partial P)} \right)_{i,j=1}^{kn}, \\ \mathbf{K} &= \left((\mathcal{K}\lambda_j, \tau_i)_{L_2(\partial P)} \right)_{i,j=1}^{kn}, & \mathbf{D} &= \left((\mathcal{D}\lambda_j, \lambda_i)_{L_2(\partial P)} \right)_{i,j=1}^{kn}.\end{aligned}$$

If we apply analogously a Galerkin formulation to the second equation in (14.11) and replace $\gamma_1 v$ by t_h on the right hand side, then we obtain the matrix

$$\mathbf{S} = \mathbf{D} + \left(\frac{1}{2} \mathbf{M}^\top + \mathbf{K}^\top \right) \mathbf{V}^{-1} \left(\frac{1}{2} \mathbf{M} + \mathbf{K} \right).$$

Because of $\gamma_0 \phi_i = \lambda_i$, the matrix entries are good approximations for

$$\mathbf{S} \approx \left((\gamma_1 \phi_j, \gamma_0 \phi_i)_{L_2(\partial P)} \right)_{i,j=1}^{kn}. \quad (14.13)$$

The entries of the matrices \mathbf{V} , \mathbf{K} and \mathbf{D} are double integrals over ∂P . The inner integral, which corresponds to the action of the boundary integral operator on a basis function, can be evaluated in closed form. The outer integral, which corresponds to the L_2 -product is approximated by numerical quadrature.

At this point, we stress that in the previous description the boundary element method is directly applied on the naturally given discretization of the polygonal element P . For example, if we have a pentagon and we are interested in $k = 1$, the Dirichlet trace is described exactly by five degrees of freedom on ∂P and the Neumann trace is approximated by one constant per edge. In general, the BEM makes use of a finer discretization of ∂P , but for our purpose the coarsest and naturally given discretization is sufficient.

Finally, we draw the connection to the global BEM-based FEM. If we compare (14.13) with (14.8) and (14.9), we see that \mathbf{S} serves as a good approximation of the local stiffness matrices in the finite element formulation. Furthermore, the approximation t_h of $\gamma_1 v$ for $v = \phi_i$ obtained by (14.12) is used in the representation formula (14.10) to evaluate the basis functions ϕ_i in the interior of the polygonal element P . All boundary element matrices are set up once per element in a BEM-based FEM simulation and are used for all basis functions. Since the number of vertices per element is bounded and we do not discretize the element boundaries further, the local BEM matrices are rather small and the inversion of \mathbf{V} can be done efficiently with a LAPACK routine.

14.2.4 Numerical examples

The theoretical results of Theorem 14.1 are illustrated on a model problem. The BEM-based FEM is applied on a sequence of uniformly refined polygonal meshes. In each step of the refinement the boundary-value problem

$$-\Delta u = f \quad \text{in } \Omega = (0, 1)^2, \quad u = 0 \quad \text{on } \Gamma$$

is solved, where f is chosen such that $u(\mathbf{x}) = \sin(\pi x) \sin(\pi y)$ is the unique solution. The initial mesh and some refinements are shown in Figure 14.1. The successively

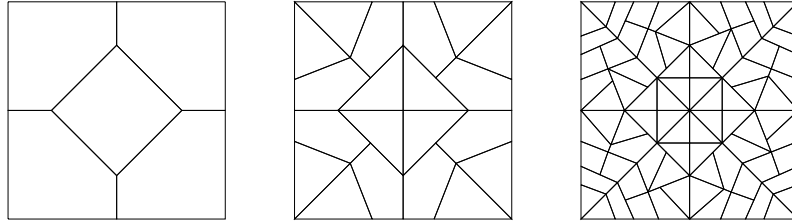


Figure 14.1 Initial mesh (left), refined mesh after two steps (middle), refined mesh after four steps (right).¹

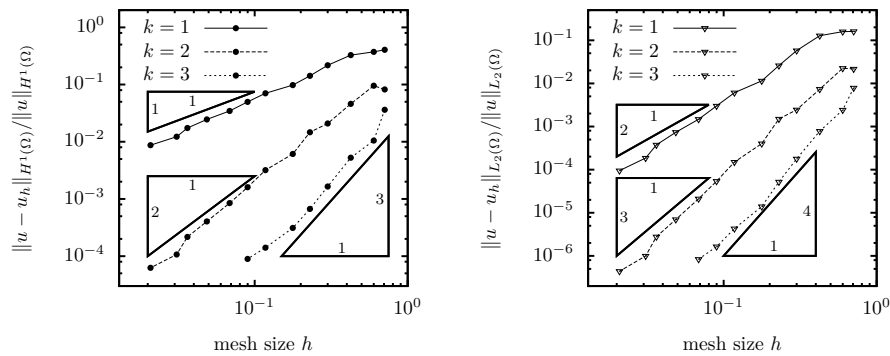


Figure 14.2 Relative error in H^1 -norm (left) and L_2 -norm (right) with respect to the mesh size h .¹

refined meshes are obtained by dividing each polygonal element as described in [17], see also the next section. The Galerkin error $\|u - u_h\|_{H^\ell(\Omega)}$ is computed for the H^1 -norm ($\ell = 1$) and the L_2 -norm ($\ell = 0$). In Figure 14.2, the relative errors are plotted with respect to the mesh size $h = \max\{h_P : P \in \mathcal{T}_h\}$ on a logarithmic scale. The slopes of the curves reflect the theoretical rates of convergence for the approximation orders $k = 1, 2, 3$.

14.3 ADAPTIVE BEM-BASED FEM IN 2D

In the uniform refinement strategy each element of the mesh is split into two new elements to obtain the next finer mesh. This splitting process is performed as described below. To obtain the optimal rates of convergence according to Theorem 14.1, the solution has to be smooth. This assumption is often violated in practical applications, where singularities can arise due to discontinuous material parameters or

¹Reprinted from Computers & Mathematics with Applications, Vol. 67(7), S. Weißer, Arbitrary order Trefftz-like basis functions on polygonal meshes and realization in BEM-based FEM, pages 1390-1406, Copyright (2014), with permission from Elsevier.

reentrant corners in the geometry. Consequently, the convergence slows down for uniform refinement. Therefore, the meshes have to be adapted to the problem in order to recover optimal rates of convergence. For the adaptive BEM-based FEM, we proceed in a common strategy, which only selects several elements for refinement in each step, see [16]. Essential ingredients are the element-wise error indicators η_P that monitor the approximation quality over the single elements. In the following we assume that these indicators bound the true error in the desired norm such that

$$\|u - u_h\| \leq c \eta_R = c \left(\sum_{P \in \mathcal{T}_h} \eta_P^2 \right)^{1/2}. \quad (14.14)$$

In Section 14.3.2, we present a residual-based error estimator, which bounds the error in the energy norm.

14.3.1 Adaptive FEM strategy

The adaptive BEM-based FEM successively refines elements that contribute most to the error. This strategy proceeds in a loop over four steps:

SOLVE The boundary-value problem (14.1) is approximated by means of the BEM-based FEM on the current polygonal mesh using the approximation space V_h^k .

ESTIMATE An error estimator η_R as well as the element-wise error indicators η_P (see Section 14.3.2) are computed on the discretization \mathcal{T}_h .

MARK A minimal subset $\mathcal{M}_h \subset \mathcal{T}_h$ of all elements are marked according to Dörflers strategy [3] such that

$$\left(\sum_{P \in \mathcal{M}_h} \eta_P^2 \right)^{1/2} \geq (1 - \theta) \eta_R,$$

where $0 \leq \theta < 1$ is a user-defined parameter. To obtain a minimal set \mathcal{M}_h , it is possible to sort the elements according to their indicators η_P and mark those with the largest indicators. Instead of that, we implemented the marking algorithm given in [3] to achieve linear complexity. Furthermore, we choose $\theta = 0.5$ in the numerical experiments.

REFINE Each marked element is refined and we consequently obtain a new mesh for the next cycle in the loop. For the refinement of an element P , we bisect P through its barycenter $\bar{\mathbf{x}}$ orthogonal to its characteristic direction, see Figure 14.3, that is given by the eigenvector that corresponds to the largest eigenvalue of the matrix

$$M_{\text{Cov}} = \int_P (\mathbf{x} - \bar{\mathbf{x}})(\mathbf{x} - \bar{\mathbf{x}})^\top d\mathbf{x}, \quad \bar{\mathbf{x}} = \frac{1}{|P|} \int_P \mathbf{x} d\mathbf{x}.$$

For more details, see [17]. Furthermore, we check the regularity of the mesh

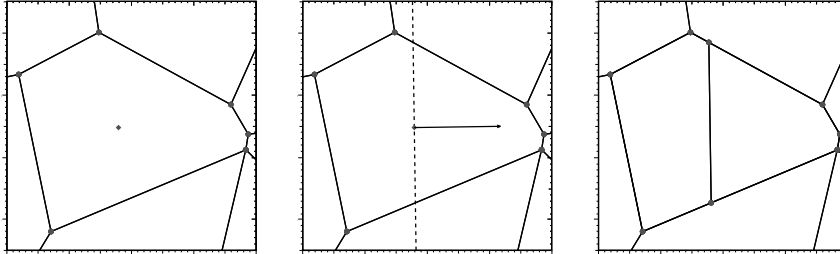


Figure 14.3 Refinement of an element: element with center $\bar{\mathbf{x}}$ (left), element with eigenvector (middle), two new elements (right).²

and refine additional elements if $c_{\mathcal{T}}h_P \leq h_{[\mathbf{v}_i, \mathbf{v}_{i+1}]}$ for any $i = 1, \dots, n$ is violated with a user-defined parameter $c_{\mathcal{T}}$.

The adaptive mesh refinement process is kept very local. Only the marked and degenerated elements are bisected during the refinement. It is not necessary to resolve hanging nodes and keep the mesh admissible as for example in the *red-blue-green* refinement procedure for triangular meshes, see [16]. This advantage is due to the polygonal meshes with very flexible elements.

14.3.2 Residual-based error estimate for polygonal meshes

The residual-based a posteriori error estimate bounds the difference of the exact solution and the Galerkin approximation in the energy norm associated to the bilinear form. Among others, the estimate contains the jumps of the conormal derivatives over the element edges. Let $P \in \mathcal{T}_h$ be a polygonal element with edge $[\mathbf{v}_i, \mathbf{v}_{i+1}]$ and $P' \in \mathcal{T}_h$ be the neighbouring element that contains this edge. Then, the jump is given on $(\mathbf{v}_i, \mathbf{v}_{i+1})$ by

$$\llbracket u_h \rrbracket = \frac{\partial u_h|_P}{\partial \mathbf{n}_P} + \frac{\partial u_h|_{P'}}{\partial \mathbf{n}_{P'}}.$$

We define the so called edge residual by

$$R_{P,i} = \begin{cases} 0 & \text{for } (\mathbf{v}_i, \mathbf{v}_{i+1}) \subset \Gamma_D, \\ g_N - \frac{\partial u_h}{\partial \mathbf{n}_P} & \text{for } (\mathbf{v}_i, \mathbf{v}_{i+1}) \subset \Gamma_N, \\ -\frac{1}{2} \llbracket u_h \rrbracket & \text{for } (\mathbf{v}_i, \mathbf{v}_{i+1}) \subset \Omega. \end{cases}$$

All ingredients are now available to state the residual-based error estimate that fulfils (14.14) for the energy norm $\|\nabla \cdot\|_{L_2(\Omega)}$.

²Reprinted from *Numerische Mathematik, Residual error estimate for BEM-based FEM on polygonal meshes*, Vol. 118, 2011, pages 765-788, S. Weißer, © Springer-Verlag 2011, with permission of Springer.

Theorem 14.2 (Reliability). *Let \mathcal{T}_h be a regular mesh. Furthermore, let $u \in V$ and $u_h \in V_h^k$ be the solutions of (14.2) and the Galerkin approximation obtained by (14.3), respectively. Then the residual-based error estimate is reliable, i.e.*

$$\|\nabla(u - u_h)\|_{L_2(\Omega)} \leq c \eta_R \quad \text{with} \quad \eta_R^2 = \sum_{P \in \mathcal{T}_h} \eta_P^2,$$

where the error indicators are defined by

$$\eta_P^2 = h_P^2 \|f + \Delta u_h\|_{L_2(P)}^2 + \sum_{i=1}^n h_{[\mathbf{v}_i, \mathbf{v}_{i+1}]} \|R_{P,i}\|_{L_2([\mathbf{v}_i, \mathbf{v}_{i+1}])}^2.$$

The constant $c > 0$ only depends on the regularity parameters of the mesh and the approximation order k .

The error in the energy norm decreases at least as fast as the error estimator η_R according to the previous theorem. In order to have a good estimator, which can be used efficiently to estimate the true error, it is important that the error does not decrease faster than η_R . This behavior is shown in the next theorem, where the error indicators η_P are bounded in terms of the error plus some data oscillations. For the lower bound, the estimate involves the neighbourhood ω_P of the element P . This patch of elements is given by $\bar{\omega}_P = \bigcup \{\bar{P}' : P' \in \mathcal{T}_h, \bar{P} \cap \bar{P}' \neq \emptyset\}$.

Theorem 14.3 (Efficiency). *Under the assumptions of Theorem 14.2, the residual-based error indicator is efficient, i.e.*

$$\eta_P \leq c \left(\|\nabla(u - u_h)\|_{L_2(\omega_P)}^2 + h_P^2 \|f - \tilde{f}\|_{L_2(\omega_P)}^2 + \sum_{\substack{i=1, \dots, n: \\ [\mathbf{v}_i, \mathbf{v}_{i+1}] \not\subset \Gamma_D}} h_{[\mathbf{v}_i, \mathbf{v}_{i+1}]} \|g_N - \tilde{g}_N\|_{L_2([\mathbf{v}_i, \mathbf{v}_{i+1}])}^2 \right)$$

where \tilde{f} and \tilde{g}_N are piecewise polynomial approximations of the data f and g_N , respectively. The constant $c > 0$ only depends on the regularity parameters of the mesh and the approximation order k .

The terms $\|f - \tilde{f}\|_{L_2(\omega_P)}$ and $\|g_N - \tilde{g}_N\|_{L_2([\mathbf{v}_i, \mathbf{v}_{i+1}])}$ are often called data oscillations. They are usually of higher order.

14.3.3 Numerical examples

Let $\Omega = ((-1, 1) \times (-1, 1)) \setminus ([0, 1] \times [0, -1])$ and $\Gamma_D = \partial\Omega$. Using polar coordinates (r, φ) for $x = (r \cos \varphi, r \sin \varphi)$, the boundary data g_D is chosen in such a way that

$$u(r \cos \varphi, r \sin \varphi) = r^{2/3} \sin\left(\frac{2\varphi}{3}\right)$$

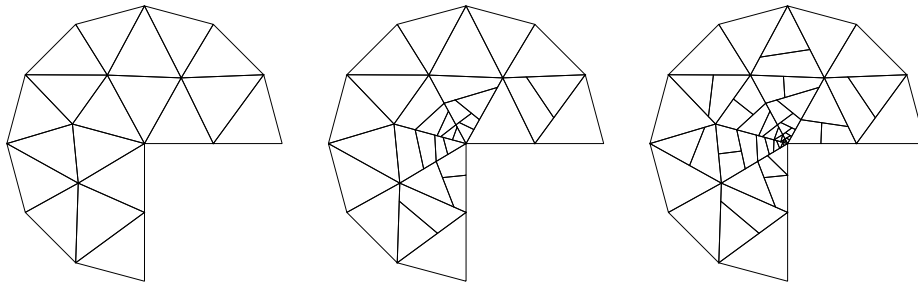


Figure 14.4 Initial mesh (left), adaptive refined mesh after five steps (middle), adaptive refined mesh after ten steps (right).²

is the solution of the boundary-value problem

$$-\Delta u = 0 \quad \text{in } \Omega, \quad u = g_D \quad \text{on } \Gamma.$$

The inhomogeneous Dirichlet data is treated by means of a discrete extension as usual in finite element methods. The boundary-value problem is discretized using the first order approximation space V_h^1 on uniformly and adaptively refined meshes. Because of the reentrant corner in the geometry, the solution does not meet the regularity assumptions of Theorem 14.1. The derivatives of u have a singularity at the origin of the coordinate system, and consequently, uniform refinement yields sub-optimal rates of convergence. However, we still expect optimal rates of convergence for the adaptive BEM-based FEM computation.

On a sequence of uniform refined meshes the following hold:

$$\text{DoFs} = \mathcal{O}(h^{-2}),$$

where DoFs denotes the number of degrees of freedom. Since the mesh size h is not strictly monotonically decreasing for adaptive refinement strategies, we study the convergence with respect to the number of degrees of freedom. Figure 14.4 shows the initial mesh as well as the adaptive meshes after five and ten refinement steps. The adaptive algorithm obviously detects the singularity and tunes the mesh towards the origin of the coordinate system. The refinement is kept very local since hanging nodes do not have to be resolved by additional refinements. The convergence plot in Figure 14.5 confirms the predicted behavior. Whereas the convergence for uniform refinement slows down, the adaptive algorithm recovers linear convergence, which corresponds to a slope of $-1/2$. Furthermore, the residual-based error estimator η_R bounds the true error and represents the reduction of the error very well, see Figure 14.5.

In order to further stress the use and the flexibility of polygonal meshes in

²Reprinted from *Numerische Mathematik, Residual error estimate for BEM-based FEM on polygonal meshes*, Vol. 118, 2011, pages 765-788, S. Weißer, © Springer-Verlag 2011, with permission of Springer.

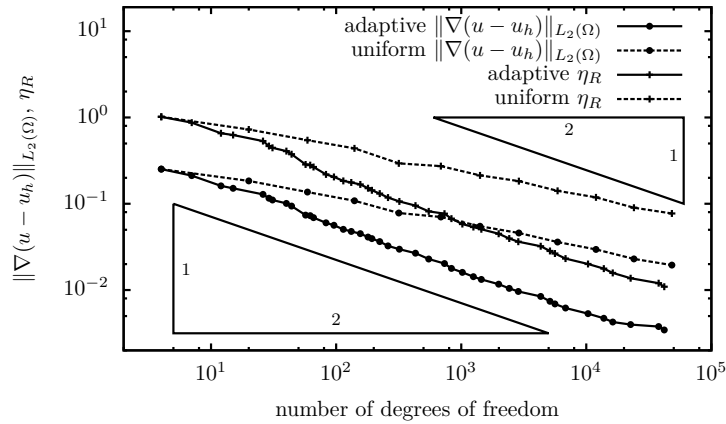


Figure 14.5 Convergence for singular solution on arc, cf. Figure 14.4, in logarithmic scale.²

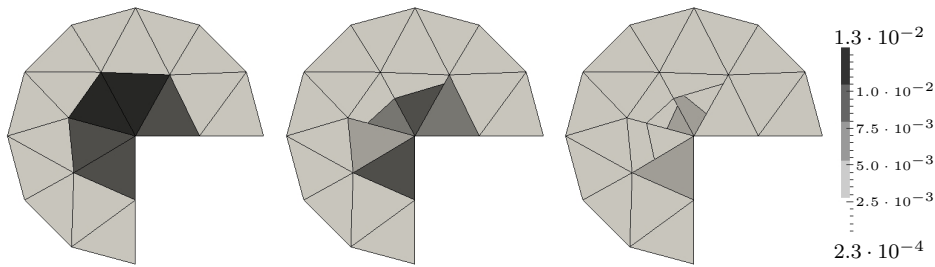


Figure 14.6 Error distribution $\|\nabla(u - u_h)\|_{L_2(P)}^2$ for the first three meshes.²

adaptive computations, we analyse the first two refinement steps. For this reason the error distribution is visualized in Figure 14.6 for the first three meshes. Each element P is colored according to the value $\|\nabla(u - u_h)\|_{L_2(P)}$. The adaptive algorithm apparently marks and refines the elements with the largest error contribution. The introduced nodes on straight edges (hanging nodes for classic meshes) are not resolved. Each of these nodes corresponds to a degree of freedom in the FE computation and thus, improves the approximation within the neighboring elements. For example, the upper right triangle close to the reentrant corner in Figure 14.6 is not refined. But, the error reduces due to the additional nodes on the left edge, namely, the triangle became a pentagon in the right most mesh.

²Reprinted from Numerische Mathematik, Residual error estimate for BEM-based FEM on polygonal meshes, Vol. 118, 2011, pages 765-788, S. Weißer, © Springer-Verlag 2011, with permission of Springer.

14.4 DEVELOPMENTS AND OUTLOOK

The idea of the BEM-based FEM has been applied to time-dependent problems [19] and in the discretization of $H(\text{div})$ -conforming approximation spaces over polygonal meshes [4]. The application in three-dimensional problems on polyhedral meshes was already discussed in the original work [2] and a generalization has been given in [13]. Additionally, a finite element tearing and interconnecting (FETI) type solver has been developed to handle the large system of linear equations [8]. In this section we present the essentials for 3D problems and provide an application to a convection-dominated boundary-value problem.

14.4.1 Hierarchical construction for 3D problems

In several publications on the BEM-based FEM the approach is applied to three-dimensional problems. For simplicity we restrict ourselves to the first order method ($k = 1$) in the following. The construction of basis functions is straightforward, as soon as it is assumed that the faces of the polyhedral elements are triangles. In the original approach, the basis functions are defined analogously to the two-dimensional case. For each vertex \mathbf{v}_i , we have a function ϕ_i such that $\phi_i(\mathbf{v}_j) = \delta_{ij}$, it is linear on the triangular faces, and ϕ_i is harmonic inside the polyhedral element. Furthermore, a three-dimensional version of the boundary element method is available. Here, the boundary integral operators only differ in their kernel function and, of course, in the integration which is done over two-dimensional surfaces of the polyhedra instead of one-dimensional boundaries of the polygons. In the treatment of the resulting boundary integral equation, in order to approximate the Neumann trace, the Sobolev spaces $H^{1/2}(\partial P)$ and $H^{-1/2}(\partial P)$ are discretized by continuous and piecewise linear polynomial functions over the surface triangles and by piecewise constant functions, respectively. All considerations on the assembling of the finite element matrix in 2D transfer to the 3D case.

What can be done in the case of general polyhedral elements with polygonal faces? An obvious and practicable idea is to triangulate the surface ∂P of the polyhedral element P first and then apply the strategy described above. However, this introduces additional and artificial vertices to the polyhedral element which lead to additional degrees of freedom in the finite element computation. An alternative approach has been proposed in [13] that is applicable on general polygonal faces.

In order to motivate the construction in 3D, we analyse once more the first order basis functions ϕ_i for $i = 1, \dots, n$ in 2D, or equivalently the harmonic coordinates from Section 1.2.8. These functions fulfil $\phi_i(\mathbf{v}_j) = \delta_{ij}$, are linear on the one dimensional edges and are harmonic inside the two-dimensional polygonal element. We observe that the second derivative of a linear function vanishes. Consequently, if we parametrize the edges linearly and treat ϕ_i as a function of one variable along the edge, we see that $\phi_i'' = 0$. Therefore, the linear function ϕ_i is harmonic in 1D on the edge and can be interpreted as solution of a Laplace problem with boundary data which is correspondingly 0 and 1. From this point of view, it is obvious how to proceed for the construction in 3D. Let Δ_1 and Δ_2 denote the one and two-

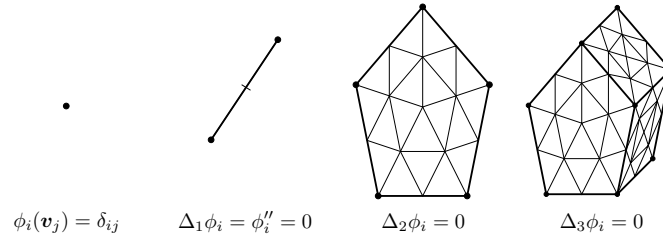


Figure 14.7 Construction of 3D basis functions for pentagonal prism P as well as auxiliary triangulation of the surface ∂P .

dimensional Laplace operators in the linear parameter spaces of an edge and face, respectively, and Δ_3 be the usual Laplace operator in three dimensions. Then, the basis functions are defined by

$$\begin{aligned} \phi_i(\mathbf{v}_j) &= \delta_{ij} & j = 1, \dots, n, \\ -\Delta_1 \phi_i &= 0 & \text{on each edge,} \\ -\Delta_2 \phi_i &= 0 & \text{on each face,} \\ -\Delta_3 \phi_i &= 0 & \text{in } P. \end{aligned}$$

This procedure is visualized in Figure 14.7, where the auxiliary triangulation of ∂P can be neglected for the definition. We prescribe the values at the vertices. Afterwards, we solve 1D Laplace problems on the edges with the given data in the vertices as boundary-values, which is equivalent to connecting the values by a linear function. Next, 2D Laplace problems are solved on each polygonal face with the previously defined data on the edges as boundary-values. And finally, the data on the faces is used as Dirichlet data for 3D Laplace problems in the element. Thus, we have a hierarchical construction for the basis functions starting from the definition at the vertices and going over the edges to the faces and finally to the elements. In the case of a polyhedral element P with triangular faces the two strategies result in the same basis functions. If we have polygonal faces, however, the hierarchical strategy has fewer basis functions compared to the original one in general.

In the realization of the approach, we have to deal with an implicit definition of basis function on faces as well as on elements. To handle these two and three-dimensional boundary-value problems, it has been proposed to introduce an auxiliary triangulation of the surface of P in [13]. For this reason the vertices of each face are connected with the center of mass of this face. The resulting triangulation can be refined successively such that several levels of nested triangular meshes are obtained. We denote the triangular mesh of the surface ∂P by $\mathcal{T}_h(\partial P)$. In Figure 14.7, $\mathcal{T}_h(\partial P)$ is shown for one successive refinement. Afterwards, the Sobolev spaces $H^{1/2}(\partial P)$ and $H^{-1/2}(\partial P)$ are discretized as usual on the surface triangulation $\mathcal{T}_h(\partial P)$, see above. The piecewise linear and continuous functions in the discrete space over $\mathcal{T}_h(\partial P)$ from the 3D BEM can be used for a 2D finite element method on each face to approximate the basis functions ϕ_i there. Consequently,

standard 2D FEM tools are used to handle the boundary-value problems on the faces and standard 3D BEM tools are applied for the problems on the element. This approach yields optimal rates of convergence for polyhedral meshes in 3D, see [13].

14.4.2 Convection-adapted basis functions in 3D

In the following we depart from the model Laplace equation and discuss the convection-diffusion equation

$$Lu = -\varepsilon\Delta u + \mathbf{b} \cdot \nabla u = 0 \quad (14.15)$$

on a bounded polyhedral domain $\Omega \subset \mathbb{R}^3$ with constant $\varepsilon > 0$, $\mathbf{b} \in \mathbb{R}^3$, $\mathbf{b} \neq 0$ and some boundary conditions. As already mentioned in the introduction, the basis functions ϕ_i are now constructed for the differential operator L . The lowest order basis functions fulfil $L\phi_i = 0$ instead of $-\Delta\phi_i = 0$ in each polyhedral element. Whereas piecewise linear functions are recovered on triangular and tetrahedral meshes for the Laplace operator, we now build-in some non-linear features of the differential operator L into the functions ϕ_i .

The original version of the BEM-based FEM is applied in [7] to (14.15) on a fixed tetrahedral mesh in 3D. Thus, the basis functions ϕ_i are linear on the surface triangles of the tetrahedral elements and fulfil the differential equation (14.15) inside the elements. The case $\varepsilon \rightarrow 0$ is numerically analysed. Standard methods without additional stabilization run into oscillations for small ε , since the equation degenerates to a first-order problem. The original BEM-based FEM formulation without explicit stabilization, however, shows less oscillations due to the built in features. The hierarchical construction described in the previous subsection even improves this effect. In this case the basis functions ϕ_i fulfil certain projected convection-diffusion equations on the edges and faces of the tetrahedra, see Figure 14.7 and replace $-\Delta$ by L . The results presented in [9] are even promising when compared to a streamline upwind/Petrov-Galerkin (SUPG) finite element method, which has explicit stabilization to treat the convection dominated case.



Bibliography

- [1] L. Beirão da Veiga, F. Brezzi, A. Cangiani, G. Manzini, L. D. Marini, and A. Russo. Basic principles of virtual element methods. *Mathematical Models and Methods in Applied Sciences*, 23(01):199–214, 2013.
- [2] D. Copeland, U. Langer, and D. Pusch. From the boundary element domain decomposition methods to local Trefftz finite element methods on polyhedral meshes. In *Domain decomposition methods in science and engineering XVIII*, volume 70 of *Lecture Notes in Computational Science and Engineering*, pages 315–322. Springer, Berlin, Heidelberg, 2009.
- [3] W. Dörfler. A convergent adaptive algorithm for Poisson’s equation. *SIAM Journal on Numerical Analysis*, 33(3):1106–1124, 1996.
- [4] Y. Efendiev, J. Galvis, R. Lazarov, and S. Weißer. Mixed FEM for second order elliptic problems on polygonal meshes with BEM-based spaces. In I. Lirkov, S. Margenov, and J. Waśniewski, editors, *Large-Scale Scientific Computing*, volume 8353 of *Lecture Notes in Computer Science*, pages 331–338. Springer, Berlin, Heidelberg, 2014.
- [5] C. Hofreither. L_2 error estimates for a nonstandard finite element method on polyhedral meshes. *Journal of Numerical Mathematics*, 19(1):27–39, 2011.
- [6] C. Hofreither, U. Langer, and C. Pechstein. Analysis of a non-standard finite element method based on boundary integral operators. *Electronic Transactions on Numerical Analysis*, 37:413–436, 2010.
- [7] C. Hofreither, U. Langer, and C. Pechstein. A non-standard finite element method for convection-diffusion-reaction problems on polyhedral meshes. *AIP Conference Proceedings*, 1404(1):397–404, 2011.
- [8] C. Hofreither, U. Langer, and C. Pechstein. FETI solvers for non-standard finite element equations based on boundary integral operators. In J. Erhel, M. Gander, L. Halpern, G. Pichot, T. Sassi, and O. Widlund, editors, *Domain Decomposition Methods in Science and Engineering XXI*, volume 98 of *Lecture Notes in Computational Science and Engineering*, pages 731–738. Springer International Publishing, 2014.
- [9] C. Hofreither, U. Langer, and S. Weißer. Convection adapted BEM-based FEM. *ZAMM. Zeitschrift für Angewandte Mathematik und Mechanik. Journal of Applied Mathematics and Mechanics*, 96(12):1467–1481, 2016.

20 ■ Bibliography

- [10] P. Joshi, M. Meyer, T. DeRose, B. Green, and T. Sanocki. Harmonic coordinates for character articulation. *ACM Transactions on Graphics*, 26(3):Article 71, 9 pages, July 2007. Proceedings of SIGGRAPH 2007.
- [11] S. E. Mousavi and N. Sukumar. Numerical integration of polynomials and discontinuous functions on irregular convex polygons and polyhedrons. *Computational Mechanics*, 47:535–554, 2011.
- [12] S. Rjasanow and S. Weißer. Higher order BEM-based FEM on polygonal meshes. *SIAM Journal on Numerical Analysis*, 50(5):2357–2378, 2012.
- [13] S. Rjasanow and S. Weißer. FEM with Trefftz trial functions on polyhedral elements. *Journal of Computational and Applied Mathematics*, 263:202–217, 2014.
- [14] O. Steinbach. *Numerical approximation methods for elliptic boundary value problems: finite and boundary elements*. Springer, New York, 2007.
- [15] N. Sukumar and A. Tabarraei. Conforming polygonal finite elements. *International Journal for Numerical Methods in Engineering*, 61(12):2045–2066, 2004.
- [16] R. Verfürth. *A posteriori error estimation techniques for finite element methods*. Numerical Mathematics and Scientific Computation. Oxford University Press, Oxford, 2013.
- [17] S. Weißer. Residual error estimate for BEM-based FEM on polygonal meshes. *Numerische Mathematik*, 118(4):765–788, 2011.
- [18] S. Weißer. Arbitrary order Trefftz-like basis functions on polygonal meshes and realization in BEM-based FEM. *Computers & Mathematics with Applications*, 67(7):1390–1406, 2014.
- [19] S. Weißer. BEM-based finite element method with prospects to time dependent problems. In E. Oñate, J. Oliver, and A. Huerta, editors, *Proceedings of the jointly organized WCCM XI, ECCM V, ECFD VI, Barcelona, Spain, July 2014*, pages 4420–4427. International Center for Numerical Methods in Engineering (CIMNE), 2014.
- [20] S. Weißer. Residual based error estimate and quasi-interpolation on polygonal meshes for high order BEM-based FEM. *Computers & Mathematics with Applications*, 73(2):187–202, 2017.